Bloch-Siegert shift in a hybrid quantum register: Quantification and compensation

Jingfu Zhang, Sagnik Saha,* and Dieter Suter
Fakultät Physik, Technische Universität Dortmund, D-44221 Dortmund, Germany

(Received 7 June 2018; revised manuscript received 31 October 2018; published 29 November 2018)

Quantum information processing relies on unitary transformations applied to specific qubits. In most cases, these gate operations are driven by alternating electromagnetic fields that are near resonant with specific transitions between eigenstates of the system Hamiltonian. For single-qubit gate operations, they should implement the operation on the target qubit, while all other qubits should be left invariant. It is typically assumed that this goal can be achieved if the amplitude of the control field is small compared to the frequency difference between the field and the transition frequency of the passive qubits. However, in many cases, even qubits whose energy-level differences are very far from the frequency of the applied control field can be affected by nonresonant effects, which are normally nonlinear in the amplitude of the control field. A typical example is the effect known as Bloch-Siegert shift. Unless these shifts are accounted for and, if possible, compensated, they can completely destroy the information contained in the quantum register. Therefore, we study this effect quantitatively in the important example of the nitrogen vacancy center in diamond and demonstrate how it can be eliminated.

DOI: 10.1103/PhysRevA.98.052354

I. INTRODUCTION

Storage and processing of information in quantum mechanical systems, known as quantum information processing [1,2], has an enormous potential for many applications where classical systems cannot provide sufficient computational power. The realization of this potential relies, amongst others, on the capability to selectively apply gate operations to specific quantum bits (qubits), without perturbing the other qubits present in the system. In most systems that are currently being studied for this type of application, the selection of the qubits is performed in frequency space: an alternating electric or magnetic field whose frequency is tuned to the transition frequency of the targeted qubit drives the target qubit in a way that can be well described by a rotation on the Bloch sphere. This type of resonant excitation works well for many different systems, such as electronic and nuclear spins, trapped atomic ions, or neutral atoms, but also engineered systems like superconducting circuits [3].

The required selectivity of this frequency-domain addressing scheme is typically assumed to work well if the Rabi frequency of the driving field is small compared to the frequency difference between the qubits. As an example, if two qubits have transition frequencies ν^A and ν^B, the Rabi frequency ν_R should fulfill the condition $|\nu_R| \ll |\nu^A - \nu^B|$—a condition that can often be fulfilled.

Hybrid quantum registers that combine the attractive properties of different types of qubits are useful for many different applications. They also pose a number of challenges, often associated with the large differences in coupling strengths between the different types of qubits. A particularly important type of such hybrid quantum registers are systems that consist of electronic and nuclear spins. The coupling strength between a spin and a magnetic field is quantified by the gyromagnetic ratio γ: $\nu_R = \gamma B_1$, where B_1 is the amplitude of the ac magnetic field. If an alternating magnetic field is used to drive the nuclear spin, the nuclear spin Rabi frequency is $\nu_R^n = \gamma_n B_1$. The same field interacts also with the electron spin, and the corresponding Rabi frequency is $\nu_R^e = |\gamma_e| B_1$, where $\gamma_e = -28$ GHz/T is the electronic gyromagnetic ratio, which is some three orders of magnitude larger than γ_n. In most cases, the condition $|\nu_R^e| \ll |\nu^e - \nu^n| \approx |\nu^e|$ is still well fulfilled and accordingly the resonant excitation of the electron spin is negligibly small, where ν^e and ν^n denote the transition frequencies of the electron and nuclear spins. However, since the nuclear spin responds only slowly to the driving field, the gate operation is also several orders of magnitude longer than the electron spin operations. For such long pulse durations, also nonresonant effects can become relevant, in particular the Bloch-Siegert (BS) shift [4–6]: this effect can be described by an effective Hamiltonian for the transition where it is observed:

$$\frac{1}{2\pi}\mathcal{H}_{BS} = \nu_{BS}\frac{\sigma_z}{2}, \tag{1}$$

where σ_z denotes the z component of the Pauli matrix and we have set $\hbar = 1$. The frequency shift

$$\nu_{BS} = \frac{\nu_R^2}{2\nu^e} \tag{2}$$

is given by the square of the Rabi frequency ν_R, divided by twice the transition frequency ν^e. It can be calculated by the Floquet formalism [5], with a dressed atom model [7] or a unitary approach [8]. The effect has been observed, e.g., in pulsed ENDOR [9], circuit quantum electrodynamics systems [10–12], and Rydberg atoms [13]. Clearly, this effect

*Present address: Indian Institute of Science Education and Research Kolkata, Mohanpur 741246, India.

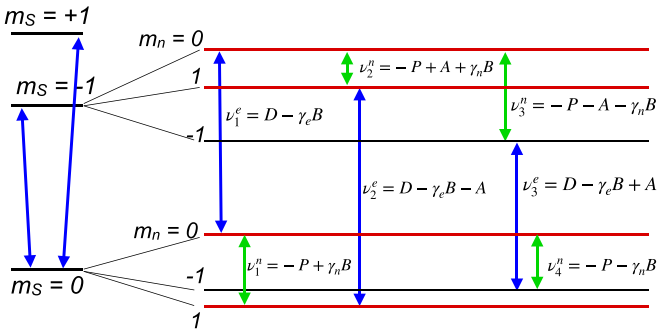

FIG. 1. Energy diagram of the NV center coupled with ^{14}N spin. The four basis states marked by thick red horizontal lines form a two-qubit system. The vertical arrows indicate the allowed ESR and NMR transitions. The transition frequencies are indicated next to the arrows.

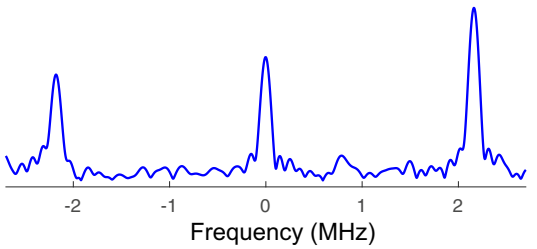

FIG. 2. Spectrum of the ESR transitions between the states with $m_S = 0$ and -1, obtained as Fourier transform of the time-domain signals. The origin of the frequency axes is set to $D - |\gamma_e|B$, measured as 2438.739 MHz. The vertical axis denotes the amplitude of the signal.

becomes large when strong pulses are used [14,15], or in the cavity-enhanced ultrastrong coupling regime [16–22]. In the case of high-fidelity quantum control, the effects are smaller but no less relevant, since they may significantly degrade the fidelity of the operations [23,24]. Here, we investigate the BS effects that radio frequency (rf) pulses have on the electron spin of a nitrogen vacancy (NV) center in diamond.

II. SYSTEM AND EXPERIMENTAL PROTOCOL

We demonstrate the issue for the example of a system consisting of the electron and ^{14}N nuclear spins in a single NV center in a ^{12}C enriched sample [25,26], with a static magnetic field B oriented along its symmetry axis. The experiments were performed at room temperature. The Hamiltonian for this system can be written as [27,28]

$$\frac{1}{2\pi}\mathcal{H} = DS_z^2 - \gamma_e B S_z + PI_z^2 - \gamma_n B I_z + AS_z I_z. \quad (3)$$

Here S_z and I_z are the z components of the spin-1 operators for electronic and nuclear spins, respectively. The zero-field splitting is $D = 2.87$ GHz, the nuclear quadrupolar splitting $P = -4.95$ MHz, the hyperfine coupling $A = -2.16$ MHz [27,29,30], and the nuclear gyromagnetic ratio $\gamma_n = 3.1$ MHz/T. In the experiments, the static field strength is about 15 mT, which results in a separation of the two electron spin resonance (ESR) transitions by about 840 MHz.

Figure 1 shows the corresponding energy-level scheme, focusing on the case where we excite the $m_S = 0 \leftrightarrow -1$ transitions of the electron spin. The ESR transition frequency was $\nu_1^e = 2438.739$ MHz, the NMR transition frequencies were $\nu_1^n = 4.990$, $\nu_2^n = 2.828$, $\nu_3^n = 7.066$, and $\nu_4^n = 4.898$ MHz, and the nuclear spin Rabi frequencies were measured as 10.7, 6.0, 6.3, and 10.4 kHz at an rf power of $p_0 \approx 80$ mW. As a minimal system for the purpose of this demonstration, we focus on the four levels marked by thick red lines, which form a two-qubit system.

Figure 2 shows the spectra of the ESR transitions between the states with $m_S = 0$ and -1, obtained in a Ramsey-type free-induction decay (FID) experiment, using resonant microwave (MW) pulses with Rabi frequencies of about 10 MHz for excitation and detection. The FID signal shows that the dephasing time (T_2^*) of the electron spin is $\approx$20 μs. The height difference of the three peaks indicates a nonzero polarization of the ^{14}N nuclear spin.

Figure 3 shows the pulse sequence used to demonstrate the effect and its compensation. During the initialization, we use a laser pulse to bring the electron spin to the $m_S = 0$ state, and then a MW pulse with a $\pi/2$ flip angle to generate coherence between the $m_S = 0$ and -1 states. This coherence allows us to observe the effect of the BS shift, which is generated by the rf pulses during the period marked as "gate" in Fig. 3. These rf pulses are required to drive gate operations on the ^{14}N nuclear spin. During the gaps in the rf pulses, we apply dynamical decoupling (DD) pulses to the electron spin, to refocus unwanted dephasing of the electron spin coherence and extend the coherence time of the electron spin. During the detection period, the MW pulse transforms the coherence to spin population and the laser pulse reads out the population of the $m_S = 0$ state $P_{|0\rangle}$.

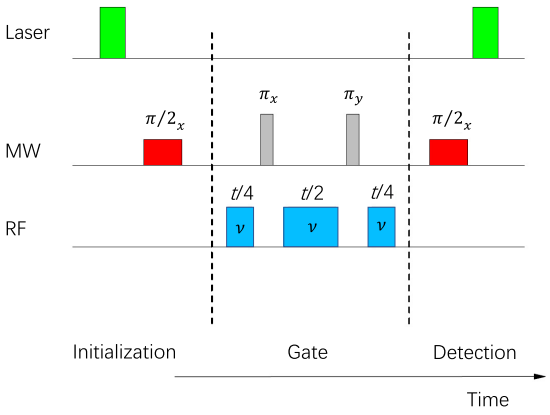

FIG. 3. Pulse sequence. The laser pulses ($\lambda = 532$ nm) are used for initialization and detection of the electron spin. The MW pulses are resonant with the transition $|0\rangle_e|0\rangle_n \leftrightarrow |-1\rangle_e|0\rangle_n$. In the initialization and detection steps, they are either transition-selective or hard pulses with Rabi frequency of about 0.30 MHz or 12 MHz. The flip angles are $\pi/2$, with the phase indicated by the index. During the gate, the MW pulses are hard pulses with Rabi frequency about 12 MHz. The frequency of the rf pulses is indicated in the rectangles.

III. MEASUREMENT OF THE FREQUENCY SHIFT

A. Observable for the BS shift

The applied rf field is oriented at an arbitrary direction with respect to the coordinate system of the NV center and has therefore components parallel as well as perpendicular to the NV axis. The parallel component, which corresponds to the z component in the conventional choice of coordinate system, leads to oscillations with the frequency of the rf field [31]. Here, we focus on the transverse components, which generate the BS shift. To quantitate the observed effect and verify the interpretation as a BS shift, we measured the dependence of the shift on the rf amplitude. For this purpose, we applied rf pulses only before the first and after the second DD pulse.

The $\pi/2$ MW pulse in the initialization step generates a superposition of the electron spin

$$|s_0\rangle = (|0\rangle - i|1\rangle)/\sqrt{2}. \tag{4}$$

The z rotation by the Hamiltonian (1) in the gate step

$$U_{BS}(t) = e^{-i2\pi\nu_{BS}t\sigma_z/4} \tag{5}$$

turns $|s_0\rangle$ into

$$|s(t)\rangle = (|0\rangle e^{-i2\pi\nu_{BS}t/4} - i|1\rangle e^{i2\pi\nu_{BS}t/4})/\sqrt{2}. \tag{6}$$

During the detection step, the second $\pi/2$ MW pulse transforms $|s(t)\rangle$ to the final state

$$|s_f(t)\rangle = |0\rangle\cos\left(2\pi\nu_{BS}\frac{t}{4}\right) + |1\rangle\sin\left(2\pi\nu_{BS}\frac{t}{4}\right), \tag{7}$$

where the population $P_{|0\rangle}$ of $|0\rangle$ encodes the BS shift. In the experiments described below, we investigate the BS shift by varying the power or the frequency of the rf field.

B. Dependence on rf power

To test the effect of the rf field, we first set the frequency far from the nuclear spin transitions and applied rf power during the first and third period of the gate in Fig. 3. In this case, the effects of the off-resonant rf field on the nuclear spin can be neglected, which simplifies the data analysis. In the initialization and detection steps, we used transition selective MW pulses with the carrier frequency set to the transition $|0\rangle_e|0\rangle_n \leftrightarrow |-1\rangle_e|0\rangle_n$. Figures 4(a)–4(d) show the experimental results for rf powers from zero to 80 mW. In the absence of an rf field, the electron spin coherence decays exponentially and we could fit the experimental data with the function

$$P_{|0\rangle} = a_1 + b_1 e^{-(t/T_2)^k}, \tag{8}$$

and obtained $T_2 = 1.3$ ms, $k = 1.2$, $a_1 = 0.40$, and $b_1 = 0.44$.

The traces of Figs. 4(a)–4(c) show the resulting signals from the electron spin, measured with a radio frequency of $\nu = 6$ MHz and rf powers of $p_0 = 80$ mW, $p_0/2$, and $p_0/4$. The data can be fitted as

$$P_{|0\rangle} = a_2 + b_2\cos\left(2\pi\frac{\nu_{BS}}{2}t\right)e^{-(t/T_2)^k}. \tag{9}$$

The resulting fit parameters are listed in Table I. Figure 4(e) shows the dependence of the measured frequency on the rf power p. According to Eq. (2), the dependence should be linear (quadratic in B_1). The line shows the theoretical prediction

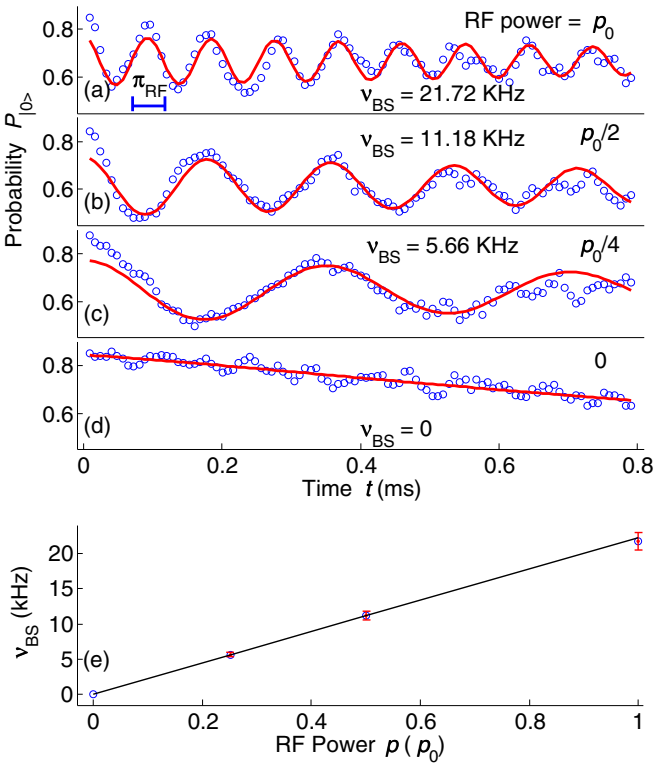

FIG. 4. Experimental results for the dependence of the BS shift on the amplitude B_1 of the rf pulses. The radio frequency was 6 MHz and the rf power was p_0, $p_0/2$, and $p_0/4$ and zero, shown as figures (a)–(d), respectively. The horizontal scale bar in the panel for rf power p_0 indicates the duration of the π pulse for the ^{14}N spin when the radio frequency is resonant with the transition at 4.990 MHz. The experimental data are shown as empty circles. Each data point corresponds to 2 M repetitions of the pulse sequence for photon collection. The fit to the data, shown as the solid curves, gave the frequencies $\nu_{BS} = 21.72$, 11.18, and 5.66 kHz. Figure (e) shows the dependence of ν_{BS} on the rf power, with the measured data as circles, and the theoretical prediction as the solid line. The error bars are estimated from the uncertainties in fitting the data in figures (a)– (c).

$\nu_{BS}^{th} = k\,p/p_0$, with $k = 22.3 \pm 0.5$. The linear correlation coefficient is 0.9999.

C. Dependence on radio frequency

In the second set of experiments, we tested the prediction of Eq. (2) that the BS shift should not depend on the radio frequency. We fixed the power of the rf pulses to p_0 and varied the frequency from 6.5 MHz to 7 and 7.5 MHz. By fitting the data using the function (9), we obtained a_2, b_2, and ν_{BS}, as

TABLE I. Fit results for a_2, b_2, and ν_{BS} in Eq. (9) obtained from the experiment data shown in Fig. 4.

rf power	a_2	b_2	ν_{BS} (kHz)
p_0	0.67	0.10	21.72
$p_0/2$	0.61	0.12	11.18
$p_0/4$	0.64	0.13	5.66

TABLE II. Fit results for a_2, b_2, and ν_{BS} in Eq. (9) obtained from the experiment data for demonstrating the dependence of the BS shift on the radio frequency, illustrated as Fig. 5, where we only showed the result for 7 MHz, since the results for 6.5, 7, and 7.5 MHz are similar.

Radio frequency (MHz)	a_2	b_2	ν_{BS} (kHz)
6.5	0.65	0.13	21.34
7.0	0.65	0.10	20.88
7.5	0.64	0.12	20.90
4.99	0.37	0.25	27.09

listed in Table II. In Fig. 5, we illustrated the result for 7 MHz. The data for the other frequencies are similar and therefore not shown in the figure. Within the experimental uncertainty, the oscillation frequency does not depend on the radio frequency, as shown in Fig. 5(c). This result agrees with the prediction of Eq. (2).

For the case that the rf pulses are resonant with the NMR transitions, they affect the nuclear as well as the electronic spin. In order to eliminate this effect and observe only the BS shift, we use hard pulses in the initialization and detection steps. In this case, we can neglect the small polarization of

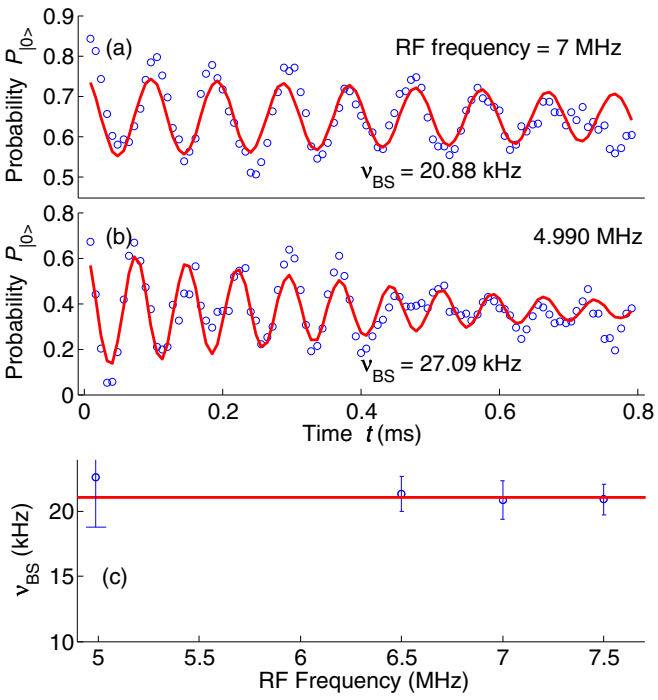

FIG. 5. Measurement of the BS shift as a function on the frequency of the rf pulses, obtained with the first and third rf pulses at power p_0. In figures (a),(b), the experimental data are shown as circles and the radio frequencies are indicated in the panels. By fitting the data, shown as the solid curves, we obtained the BS shift indicated in the panel. In figure (c), we show the measured BS shift by the empty circles for radio frequencies 6.5, 7, and 7.5 MHz. The solid line shows the average and the error bar shows the standard deviation. Since the rf power was not constant as a function of frequency, we normalized the shift observed at 4.990 MHz to the same rf power as the others.

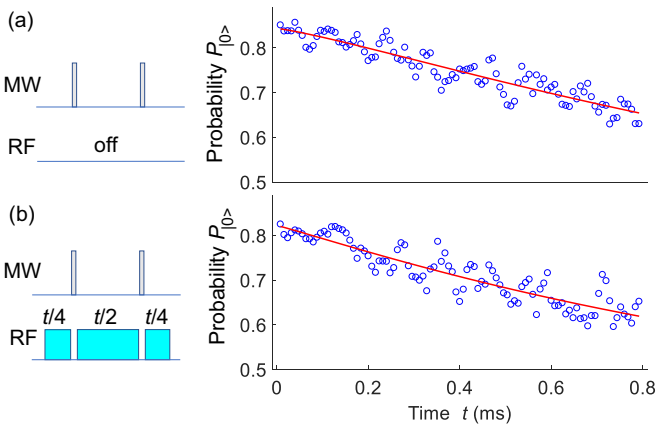

FIG. 6. Cancellation of the BS shift by DD pulses, indicated by the gray narrow rectangles. The experimental data are indicated by the empty circles, and the fits with Eq. (8) by solid curves. (a) Without rf: no shift, decay of the coherence with $T_2 = 1.3$ ms, and $k = 1.2$. (b) All the rf pulses in the sequence are switched on and have the same frequency (6 MHz) and power p_0. The experimental data can be fitted with $T_2 = 1.2$ ms and $k = 1.1$.

the nuclear spin, shown as the small difference in the peak amplitudes of Fig. 2. We applied rf pulses with frequency $\nu = \nu_1^n = 4.990$ MHz. The results are shown in Fig. 5. Table II shows the fit parameters for function (9). In this experiment, we used hard pulses for generating and detecting the electron spin coherence. Accordingly, the electron spin coherence is generated for all three subspaces of the ^{14}N spin ($m_n = 0, \pm 1$) and the observed contrast is significantly larger than in the earlier experiments, where the transition selective MW pulses affected only the subspace of $m_n = 0$. The deviation of ν_{BS} from the results in the off-resonant case can be mainly attributed to the difference of the powers. We therefore normalized the measured ν_{BS} to the applied power; the result is shown in Fig. 5(c). It is close to the average value measured in the off-resonant case. The larger error bar in the case of on-resonant fields may be attributed to the polarization of the nuclear spin, making the effects of the fields on the nuclear spin observable and interfering with the BS shift.

IV. COMPENSATION

Since the BS shift corresponds to a quasistatic shift of the resonance frequency, it can be eliminated by applying refocusing pulses, provided it is constant for the whole period. For this demonstration, we use a very simple DD sequence consisting of one π_x and one π_y pulse, as shown in Fig. 3. The total phase generated by the rf pulses, which are applied only between the DD pulses, is then $\phi_{BS} = \phi_1 - \phi_2 + \phi_3$, where the three terms denote the phase acquired before the first, between the two, and after the second DD pulse. If the rf power is constant and the relative pulse durations are 1:2:1, the total phase vanishes, $\phi_{BS} = 0$.

In Fig. 6, we illustrate the experimental results in the case of off-resonant rf pulses with power p_0 and frequency $\nu = 6$ MHz, and compare it to the case without rf. In both cases, we observe no oscillations, indicating that the phases generated by the different pulses cancel each other completely. We

can use function (8) to fit the nonoscillatory data, and obtained the fitted $T_2 = 1.2$ and 1.3 ms for data with and without rf pulses. The similarity between the results with and without rf pulses shows the good cancellation of the BS shift, consistent with the prediction in previous work [31], that the refocusing pulses embedded in the rf should also compensate the BS shift.

V. DISCUSSION

Our experiment results show clearly that the BS shift can be higher than the Rabi frequencies of the nuclear spin. This means that the BS shift should be seriously considered and the compensation is essential for implementing the control of nuclear spins by rf pulses. Furthermore, the present analysis may be useful in other contexts: from the BS shift, one can determine the amplitude (B_1) of the rf field [32] and from that the expected Rabi frequencies for arbitrary nuclear spins can be obtained as $\nu_R = \gamma B_1$. These calculated Rabi frequencies should then be considered reference values for the corresponding nuclei, since the tabulated gyromagnetic ratios are always given for standard compounds where the nuclei are in a diamagnetic environment. In the systems considered here, the hyperfine interaction can result in significantly different effective gyromagnetic ratios [28,33,34]. Accordingly, the comparison of the measured Rabi frequency with the one calculated from BS shift and reference gyromagnetic ratio can be used to obtain useful information on the elements of the hyperfine tensor that are not directly observable in the spectrum, such as the perpendicular component $A_\perp$ of the ^{14}N hyperfine coupling [33].

VI. CONCLUSION

In conclusion, we have demonstrated that ac magnetic fields that are used to drive the nuclear spins in a hybrid quantum register can have a large effect on the electronic spin, although their frequency is very far from their resonance frequencies. The main effect is a phase shift, which can easily exceed 2π and therefore completely scramble the quantum information stored in the electron spin qubit, unless measures are taken to eliminate its effect. The purpose of this work was to quantitatively measure the effect and test schemes for compensation. We have analyzed the dependence of the BS shift on the power and frequency of the rf pulses and demonstrated that spin echoes can refocus the BS effect with excellent precision. This is useful not only for compensating the effect in experiments where it perturbs the system, it can also be used, e.g., for measuring or calibrating the strength of nonresonant ac magnetic fields.

ACKNOWLEDGMENTS

This work was supported by the DFG through Grants No. SU 192/34-1 and No. SU 192/19-2. S.S. acknowledges the support by DAAD-WISE 2017 for financing his travel and stay in Germany to carry out the research project. We also thank Dr. Swathi Hegde and Ji Bian for useful discussions.

[1] M. A. Nielsen and I. L. Chuang, *Quantum Computation and Quantum Information* (Cambridge University Press, Cambridge, UK, 2000).
[2] J. Stolze and D. Suter, *Quantum Computing: A Short Course from Theory to Experiment*, 2nd ed. (Wiley-VCH, Berlin, 2008).
[3] T. D. Ladd, F. Jelezko, R. Laflamme, Y. Nakamura, C. Monroe, and J. L. O'Brien, Nature (London) **464**, 45 (2010).
[4] F. Bloch and A. Siegert, Phys. Rev. **57**, 522 (1940).
[5] J. H. Shirley, Phys. Rev. **138**, B979 (1965).
[6] L. Emsley and G. Bodenhausen, Chem. Phys. Lett. **168**, 297 (1990).
[7] C. Cohen-Tannoudji, J. Dupont-Roc, and C. Fabre, J. Phys. B **6**, L214 (1973).
[8] Y. Yan, Z. Lü, and H. Zheng, Phys. Rev. A **91**, 053834 (2015).
[9] M. Mehring, P. Höfer, and A. Grupp, Phys. Rev. A **33**, 3523 (1986).
[10] P. Forn-Diaz, J. Lisenfeld, D. Marcos, J. J. Garcia-Ripoll, E. Solano, C. J. P. M. Harmans, and J. E. Mooij, Phys. Rev. Lett. **105**, 237001 (2010).
[11] A. Baust, E. Hoffmann, M. Haeberlein, M. J. Schwarz, P. Eder, J. Goetz, F. Wulschner, E. Xie, L. Zhong, F. Quijandria *et al.*, Phys. Rev. B **93**, 214501 (2016).
[12] I. Pietikainen, S. Danilin, K. S. Kumar, A. Vepsalainen, D. S. Golubev, J. Tuorila, and G. S. Paraoanu, Phys. Rev. B **96**, 020501 (2017).
[13] D. Fregenal, E. Horsdal-Pedersen, L. B. Madsen, M. Forre, J. P. Hansen, and V. N. Ostrovsky, Phys. Rev. A **69**, 031401 (2004).
[14] K. R. K. Rao and D. Suter, Phys. Rev. A **95**, 053804 (2017).
[15] L. S. Bishop, J. M. Chow, J. Koch, A. A. Houck, M. H. Devoret, E. Thuneberg, S. M. Girvin, and R. J. Schoelkopf, Nat. Phys. **5**, 105 (2009).
[16] A. Moroz, Ann. Phys. (NY) **340**, 252 (2014).
[17] G. Gunter, A. A. Anappara, J. Hees, A. Sell, G. Biasiol, L. Sorba, S. D. Liberato, C. Ciuti, A. Tredicucci, A. Leitenstorfer *et al.*, Nature (London) **458**, 178 (2009).
[18] T. Niemczyk, F. Deppe, H. Huebl, E. P. Menzel, F. Hocke, M. J. Schwarz, J. J. Garcia-Ripoll, D. Zueco, T. Hummer, E. Solano *et al.*, Nat. Phys. **6**, 772 (2010).
[19] P. Forn-Diaz, J. J. Garcia-Ripoll, B. Peropadre, J.-L. Orgiazzi, M. A. Yurtalan, R. Belyansky, C. M. Wilson, and A. Lupascu, Nat. Phys. **13**, 39 (2017).
[20] F. Yoshihara, T. Fuse, S. Ashhab, K. Kakuyanagi, S. Saito, and K. Semba, Nat. Phys. **13**, 44 (2017).
[21] J. Braumuller, M. Marthaler, A. Schneider, A. Stehli, H. Rotzinger, W. Martin, and A. V. Ustinov, Nat. Commun. **8**, 779 (2017).
[22] J. Tuorila, M. Silveri, M. Sillanpaa, E. Thuneberg, Y. Makhlin, and P. Hakonen, Phys. Rev. Lett. **105**, 257003 (2010).
[23] M. Steffen, L. M. K. Vandersypen, and I. L. Chuang, J. Magn. Reson. **146**, 369 (2000).
[24] C. A. Ryan, C. Negrevergne, M. Laforest, E. Knill, and R. Laflamme, Phys. Rev. A **78**, 012328 (2008).
[25] J. Zhang and D. Suter, Phys. Rev. Lett. **115**, 110502 (2015).

[26] T. Teraji, T. Taniguchi, S. Koizumi, Y. Koide, and J. Isoya, Appl. Phys. Exp. **6**, 055601 (2013).
[27] C. S. Shin, M. C. Butler, H.-J. Wang, C. E. Avalos, S. J. Seltzer, R.-B. Liu, A. Pines, and V. S. Bajaj, Phys. Rev. B **89**, 205202 (2014).
[28] D. Suter and F. Jelezko, Prog. Nucl. Magn. Reson. Spectrosc. **98-99**, 50 (2017).
[29] X.-F. He, N. B. Manson, and P. T. H. Fisk, Phys. Rev. B **47**, 8816 (1993).
[30] B. Yavkin, G. Mamin, and S. Orlinskii, J. Magn. Reson. **262**, 15 (2016).
[31] M. Hirose and P. Cappellaro, Nature (London) **532**, 77 (2016).
[32] L. I. Sacolick, F. Wiesinger, I. Hancu, and M. W. Vogel, Magn. Reson. Med. **63**, 1315 (2010).
[33] M. Chen, M. Hirose, and P. Cappellaro, Phys. Rev. B **92**, 020101 (2015).
[34] K. R. K. Rao and D. Suter, Phys. Rev. B **94**, 060101 (2016).